

1                   **Improvement of short-term forecasting**  
2                   **in the Northwest Pacific through assimilating Argo**  
3                   **data into initial fields**

4  
5                   FU Hongli<sup>1</sup>, Peter C. Chu<sup>2</sup>, HAN Guijun<sup>1\*</sup>, HE Zhongjie<sup>1</sup>, LI Wei<sup>1</sup>, ZHANG Xuefeng<sup>1</sup>

6                   1 Key Laboratory of Marine Environmental Information Technology, State Oceanic  
7                   Administration, National Marine Data and Information Service, Tianjin 300171, China

8                   2 Naval Ocean Analysis and Prediction (NOAP) Laboratory

9                   Naval Postgraduate School, Monterey, CA, USA

10  
11  
12  
13  
14  
15  
16

---

\*Corresponding author

Address: 93 Liuwei Road, Hedong District, Tianjin 300171, China.

Email: fhlkjj@163.com

## Report Documentation Page

*Form Approved*  
*OMB No. 0704-0188*

Public reporting burden for the collection of information is estimated to average 1 hour per response, including the time for reviewing instructions, searching existing data sources, gathering and maintaining the data needed, and completing and reviewing the collection of information. Send comments regarding this burden estimate or any other aspect of this collection of information, including suggestions for reducing this burden, to Washington Headquarters Services, Directorate for Information Operations and Reports, 1215 Jefferson Davis Highway, Suite 1204, Arlington VA 22202-4302. Respondents should be aware that notwithstanding any other provision of law, no person shall be subject to a penalty for failing to comply with a collection of information if it does not display a currently valid OMB control number.

1. REPORT DATE <b>2012</b>	2. REPORT TYPE	3. DATES COVERED <b>00-00-2012 to 00-00-2012</b>	
4. TITLE AND SUBTITLE <b>Improvement of short-term forecasting in the Northwest Pacific through assimilating Argo data into initial fields</b>		5a. CONTRACT NUMBER	
		5b. GRANT NUMBER	
		5c. PROGRAM ELEMENT NUMBER	
6. AUTHOR(S)		5d. PROJECT NUMBER	
		5e. TASK NUMBER	
		5f. WORK UNIT NUMBER	
7. PERFORMING ORGANIZATION NAME(S) AND ADDRESS(ES) <b>Naval Postgraduate School, Naval Ocean Analysis and Prediction (NOAP) Laboratory, Monterey, CA, 93943</b>		8. PERFORMING ORGANIZATION REPORT NUMBER	
9. SPONSORING/MONITORING AGENCY NAME(S) AND ADDRESS(ES)		10. SPONSOR/MONITOR'S ACRONYM(S)	
		11. SPONSOR/MONITOR'S REPORT NUMBER(S)	
12. DISTRIBUTION/AVAILABILITY STATEMENT <b>Approved for public release; distribution unlimited</b>			
13. SUPPLEMENTARY NOTES <b>Acta Oceanologica Sinica, Chinese Society of Oceanography, in press</b>			
14. ABSTRACT <b>The impact of assimilating Argo data into initial field on the short-term forecasting accuracy of temperature and salinity is quantitatively estimated by using a forecasting system of the western North Pacific, on the base of the Princeton Ocean Model with generalized coordinate system (POMgcs). This system uses a sequential multi-grid three-dimensional variational (3DVAR) analysis scheme to assimilate observation data. Two numerical experiments were conducted with and without Argo temperature and salinity profile data besides conventional temperature and salinity profile data and sea surface height anomaly (SSHa) and sea surface temperature (SST) in the process of assimilating data into initial fields. The forecast errors are estimated through using independent temperature and salinity profiles during the forecasting period, including the vertical distributions of the horizontally averaged root mean square errors (H-RMSEs) and horizontal distributions of the vertically averaged mean errors (MEs) and temporal variation of spatially averaged root mean square errors (S-RMSEs). Comparison between the two experiments shows that the assimilation of Argo data significantly improves the forecast accuracy, with 24% reduction of H-RMSE maximum for the temperature, and the salinity forecasts are improved more obviously, averagely dropping of 50% for H-RMSEs in depth shallower than 300m. Such improvement is caused by relatively uniform sampling of both temperature and salinity from the Argo drifters in time and space.</b>			
15. SUBJECT TERMS			
16. SECURITY CLASSIFICATION OF:			17. LIMITATION OF ABSTRACT <b>Same as Report (SAR)</b>
a. REPORT <b>unclassified</b>	b. ABSTRACT <b>unclassified</b>	c. THIS PAGE <b>unclassified</b>	
			18. NUMBER OF PAGES <b>31</b>
			19a. NAME OF RESPONSIBLE PERSON



17 **Abstract**

18       The impact of assimilating Argo data into initial field on the short-term  
19 forecasting accuracy of temperature and salinity is quantitatively estimated by using a  
20 forecasting system of the western North Pacific, on the base of the Princeton Ocean  
21 Model with generalized coordinate system (POMgcs). This system uses a sequential  
22 multi-grid three-dimensional variational (3DVAR) analysis scheme to assimilate  
23 observation data. Two numerical experiments were conducted with and without Argo  
24 temperature and salinity profile data besides conventional temperature and salinity  
25 profile data and sea surface height anomaly (SSHa) and sea surface temperature (SST)  
26 in the process of assimilating data into initial fields. The forecast errors are estimated  
27 through using independent temperature and salinity profiles during the forecasting  
28 period, including the vertical distributions of the [horizontally averaged root mean](#)  
29 [square errors \(H-RMSEs\)](#) and horizontal distributions of the vertically averaged mean  
30 errors (MEs) and temporal variation of spatially averaged [root mean square errors](#)  
31 [\(S-RMSEs\)](#). Comparison between the two experiments shows that the assimilation of  
32 Argo data significantly improves the forecast accuracy, with 24% reduction of  
33 [H-RMSE](#) maximum for the temperature, and the salinity forecasts are improved more  
34 obviously, averagely dropping of 50% for [H-RMSEs](#) in depth shallower than 300m.  
35 Such improvement is caused by relatively uniform sampling of [both temperature and](#)  
36 [salinity from the Argo drifters](#) in time and space.

37 Key words: Data assimilation, Argo data, Western North Pacific, Ocean prediction

## 38 **1. Introduction**

39 Data assimilation, required in operational ocean data retrieval, has contributed  
40 significantly to the success of ocean prediction. It is to blend modeled variable ( $x_m$ )  
41 with observational data ( $y_o$ ) (Chu et al., 2004; Chu et al., 2010),

$$42 \quad x_a = x_m + W \bullet [y_o - H(x_m)] \quad (1)$$

43 where  $x_a$  is the assimilated variable; H is an operator that provides the model's  
44 theoretical estimate of what is observed at the observational points, and W is the  
45 weight matrix. Difference among various data assimilation schemes such as optimal  
46 interpolation (Chu et al., 2007a; Chu et al., 2007b), Kalman filter (Galanis et al.,  
47 2011), and three-dimensional variational (3DVAR) methods (Li et al., 2008) is the  
48 different ways to determine the weight matrix W. The data assimilation process (1)  
49 can be considered as the average (in a generalized sense) of  $x_m$  and  $y_o$ . The two parts  
50 ( $x_m$  and  $y_o$ ) in the assimilation process usually have very different characteristics in  
51 terms of data temporal and spatial distribution: uniform and dense in the modeled data  
52 ( $x_m$ ), and non-uniform and sparse in the observed data ( $y_o$ ). Question arises: What is  
53 the impact of data sampling strategies in the assimilation of initial field on the  
54 forecasting accuracy? To answer this question, two observational datasets are needed  
55 with different types of data distribution patterns in space and time. One is relatively  
56 uniform, and the other is not.

57 The Global Temperature and Salinity Profile Program (GTSP), as a cooperative  
58 international project, has been established since 1990 to provide global temperature (T)

59 and salinity (S) resources. GTSP contains conventional temperature and salinity  
60 profile data such as Nansen bottle, conductivity-temperature-depth (CTD), and  
61 bathythermograph (BT), which are usually collected from ships. Since the Array for  
62 Real-time Geostrophic Oceanography (Argo) is launched into practice, GTSP (T, S)  
63 profiles increase rapidly in both quantity and quality. It becomes possible to monitor  
64 the temporal and spatial variations of temperature and salinity simultaneously. Liu et  
65 al. (2004) showed significant improvement of temperature prediction in the central  
66 Pacific using a global ocean model with Argo data assimilation. Griffa et al. (2006)  
67 analyzed the impact of Argo data assimilation on a Mediterranean prediction model  
68 by a set of idealized experiments, and discussed the impact of coverage density and  
69 locations of Argo data on assimilation results.

70 Due to the limitation of ship time, the conventional (T, S) profile data are  
71 non-uniformly distributed in space and time. However, the Argo floats drift freely  
72 with ocean currents, the Argo data are more uniformly distributed in space and time  
73 than the conventional data. Such difference in data distributions between the  
74 conventional (non-uniform) and Argo (relatively uniform) (T, S) profile data provides  
75 an opportunity to study the effect of the sampling strategies on the ocean prediction  
76 accuracy. To do so, a numerical forecasting system with 3DVAR in the western  
77 Pacific regional seas (Fig. 1) is constructed with the capability to assimilate sea  
78 surface height anomaly (SSHa) from altimeters and sea surface temperature (SST)  
79 from satellite remote sensors, as well as in-situ conventional and Argo (T, S) profiles  
80 in the determining of the initial conditions. A seven-day forecast is conducted with

81 and without the assimilation of Argo (T, S) profiles in initial field. The prediction  
82 accuracy is verified with independent temperature and salinity profiles during the  
83 period of prediction (not used in the data assimilation of initial field). Difference  
84 between the two forecast experiments shows the impact of data distribution on the  
85 ocean prediction accuracy.

86 Frame of the paper is outlined as follows. Section 2 shows the basic features of  
87 conventional and Argo profile data. Section 3 describes the ocean dynamic model and  
88 ocean data assimilation scheme. Section 4 gives the experiment design and the  
89 quantitative analysis on the improvement of ocean prediction using the Argo data  
90 assimilation. Section 5 presents the conclusions.

91  Figure 1

## 92 **2. Data**

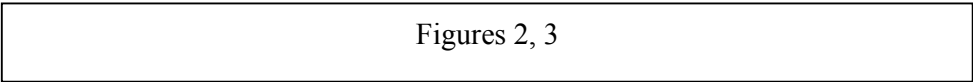
93 Ocean observational Data (January-December 2008) include SSHa from  
94 multi-satellite altimeters and SST from satellite remote sensors, and (T, S) profiles  
95 (conventional and Argo) from GTSPP. The satellite SSHa and SST data are on the  
96 horizontal resolution of  $0.25^\circ$  and the time increment of 1 day. Quality control is  
97 conducted on both conventional and Argo profile data before assimilating them into  
98 the initial field of the numerical forecasting. For the conventional data, it includes  
99 position/time check, depth duplication check, depth inversion check, temperature and  
100 salinity range check, excessive gradient check, and stratification stability check. For

101 the Argo floats, it includes duplicate float test, land position test, float drafting  
102 velocity test, pressure range test, temperature and salinity coherence test, pressure  
103 level duplication test and pressure inversion test, spike test, salinity and temperature  
104 gradient test, and stratification stability test, etc. In addition, the calibration method  
105 developed by Wong et al. (2003) is employed to calibrate the sensor drift of salinity  
106 measurements in the Argo data.

107 Figure 2 shows the horizontal distribution of (T, S) profile data. From January to  
108 December 2008, there are 60634 temperature profiles and 52638 salinity profiles from  
109 conventional observations, 5323 temperature profiles and 5210 salinity profiles from  
110 Argo floats. That is to say, the Argo data is near 1/10 of the conventional data. The  
111 conventional (T, S) profiles are distributed non-uniformly in horizontal with most  
112 profiles around Japan and east of Taiwan and much less profiles in the other regions,  
113 and existence of some data-void areas. The Argo (T, S) profiles are distributed  
114 uniformly (relative) over the whole area. Figure 3 shows the vertical distributions of  
115 numbers of observations for temperature and salinity from conventional and Argo data.  
116 The conventional temperature (salinity) observations decrease slowly from 57597  
117 (48595) data points near the surface to about 40000 (T and S) data points at near 700  
118 m depth, and reduce drastically to around 2000 (T and S) data points below 700 m  
119 depth (Fig. 3a). The Argo temperature (salinity) observations have 5299 (5186) data  
120 points from near surface to about 420 m depth, decrease almost linearly to 2000 (T  
121 and S) data points at about 1500 m depth, keep 2000 (T and S) data points from 1500  
122 to 1800 m depth, and reduce to less than 100 data points at 2000 m depth (Fig. 3b).



123 Two (T, S) datasets are used to investigate the impact of the sampling strategies  
124 on the ocean prediction accuracy. The first dataset (called “WITH\_ARGO”) contains  
125 Argo profile data besides conventional profiles, SSHa and SST and represents  
126 horizontally uniform (relative) sampling. The second dataset (called “NO\_ARGO”)  
127 contains only the conventional profile data, SSHa and SST and represents horizontally  
128 non-uniform sampling.

129  Figures 2, 3

### 130 **3. Ocean Prediction System**

#### 131 **3.1 Ocean Model**

132 The ocean model used in this study is the Princeton Ocean Model with  
133 generalized coordinate system (POMgcs). The study domain covers from 99°E to  
134 150°E in longitude, and from 10°N to 52°N in latitude (Fig. 1), with variable  
135 horizontal resolution starting from 1/12° near the coastal waters of China and  
136 Kuroshio, and telescoping to 1/2° at other areas. The vertical coordinate is a  
137 combination of sigma and z-level with a maximum depth of 5035 m, discretized by 35  
138 model levels. In the vicinity of upper mixed layer and thermocline, z-coordinate is  
139 adopted in order to get a higher vertical resolution. In shallow water and the area near  
140 bottom boundary, the terrain-following  $\sigma$ -coordinate is used. Sea surface forcing  
141 fields consist of winds, air temperatures, humidity and clouds from the National  
142 Centers for Environmental Prediction (NCEP) reanalysis. Sea surface heat fluxes are

143 calculated by bulk formula, and open boundary conditions are provided by the  
144 simulation results of Massachusetts Institute of Technology general circulation model  
145 (MITgcm, Marshall et al., 1997), including daily Sea level, temperature, salinity, and  
146 currents. These open boundary data are interpolated to the grid and time step of the  
147 forecasting system.

### 148 **3.2 Ocean Data Assimilation Scheme**

149 The ocean data assimilation scheme used in the system is a sequential  
150 three-dimensional variational (3DVAR) analysis scheme designed to assimilate  
151 temperature and salinity using a multi-grid framework (Li et al., 2008). This  
152 sequential 3DVAR analysis scheme can be performed in three dimensional spaces and  
153 can retrieve resolvable information from longer to shorter wavelengths for a given  
154 observation network and yield multi-scale analysis. The basic idea of this data  
155 assimilation scheme can be referred to Li et al. (2008) and Li et al. (2010).

156 The data assimilation is carried out in the upper 1000m. The basic idea proposed  
157 by Troccoli et al. (2002) is employed to make salinity adjustment for the background  
158 field after temperature data is assimilated. The area extent of adjustment is limited  
159 between the latitude of 30°S-30°N and depth of 50-1000m. It needs firstly to establish  
160 a T-S relationship by using interpolation algorithm based on the instant model T-S  
161 table. Then the background field of salinity is adjusted based on the T-S relationship  
162 and temperature analysis result. In addition, an idea of converting satellite altimeter  
163 SSHa into T-S “pseudo profiles” based on the 3DVAR scheme is adapted ((Zhu and

164 Yan, 2006; He et al., 2010).

165 Figure 4 shows the flow chart for data assimilation procedure: (1) Based on 24-h  
166 forecasting (T, S) values, obtain the T-S relationship at every grid point through using  
167 the T-S relationship module; (2) Convert altimeter SSHa into “pseudo profiles” of  
168 temperature and salinity; (3) Assimilate temperature data to obtain temperature  
169 analysis field; (4) Adjust 24-h forecasting salinity field on the base of the T-S  
170 relationship and temperature analysis result, and take the adjusted salinity field as the  
171 background field for salinity assimilation; (5) Assimilate salinity data to obtain  
172 salinity analysis field; (6) the temperature and salinity analysis fields are used as the  
173 initial conditions of next seven-day forecast.

174  Figure 4

### 175 **3.3. Experiment Design**

176 Two forecast experiments are designed. The first experiment (called  
177 “NO\_ARGO”) assimilates all available observations (conventional *T*, *S* profiles and  
178 SSHa and SST) except the Argo profile data. The second experiment (called  
179 “WITH\_ARGO”) assimilates all available observations including the Argo profile  
180 data. Both experiments use the same sea-surface forcing fields and open boundary  
181 conditions. The China Ocean ReAnalysis (CORA) fields of January 1, 2008 (Han et  
182 al., 2011, <http://www.cora.net.cn>) are used as initial conditions. First, a seven-day  
183 forecast is performed for both experiments. Second, the data assimilation is performed  
184 using 24-hour forecast values as the background field. Taking the assimilated fields as

185 initial conditions, the next seven-day forecast is performed. This procedure  
186 (forecast-assimilation-forecast) is cycled 365 times to obtain 24-hour, 48-hour,  
187 72-hour, 96-hour, 120-hour, 144-hour, 168-hour forecast values of temperature and  
188 salinity fields in every day of 2008. The time window of assimilating SST and SSHa  
189 data in both experiments is set to one day, namely assimilating satellite data within the  
190 one day before initial forecasting time. Since the spatial distributions of conventional  
191 observations and Argo data are sparse, both experiments adopt the 3.5-day time  
192 window, namely assimilating ocean ( $T$ ,  $S$ ) profile data within the 3.5 days before  
193 initial forecasting time. Since all temperature and salinity observational data during  
194 the period of forecasting are not assimilated into background fields (initial field of the  
195 numerical forecasting), they are taken as independent data to be used to check the  
196 forecast result. Based on these independent observation data, the errors of the 24-hour,  
197 48-hour, 72-hour, 96-hour, 120-hour, 144-hour, and 168-hour forecast values of the  
198 temperature and salinity at each grid point in every day of 2008 can be estimated. The  
199 vertical distributions of forecast errors are obtained by averaging the errors in the  
200 horizontal direction. The horizontal distributions of forecast errors are obtained by  
201 averaging the errors in the vertical direction. Difference of forecast errors between the  
202 two experiments shows the effect of sampling strategies on the ocean prediction  
203 accuracy.

## 204 4. Effect of Argo Data

### 205 4.1 Whole 3D Domain

206 To quantify the impact of assimilating Argo data on an ocean prediction errors,  
207 the [horizontally averaged root mean square error \(H-RMSE\)](#) between predicted and  
208 observed values for the whole horizontal region at depth  $z_k$  and time  $t_m$  is calculated  
209 by

$$210 \quad \text{H-RMSE}^{(\psi)}(z_k, t_m) = \sqrt{\frac{1}{N} \sum_{n=1}^N [\psi^p(x_n, y_n, z_k, t_m) - \psi^o(x_n, y_n, z_k, t_m)]^2} \quad (2)$$

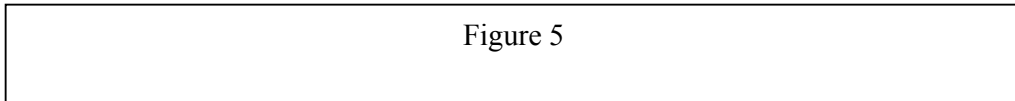
211 where  $x_n$  and  $y_n$  indicate the zonal and latitudinal coordinates of the  $n$ th observation  
212 point, respectively;  $z_k$  is the depth of the  $k$ th level;  $t_m$  is the  $m$ th forecasting time;  $N$  is  
213 total number of observation points at the  $t_m$  time and  $z_k$  depth;  $\psi^p(x_n, y_n, z_k, t_m)$  and  
214  $\psi^o(x_n, y_n, z_k, t_m)$  respectively denote the predicted and ground-truth values at the  $t_m$   
215 time and  $z_k$  depth for the point  $(x_n, y_n)$ . In the study,  $\psi$  indicates temperature ( $T$ ) or  
216 salinity ( $S$ ).  $\text{H-RMSE}^{(\psi)}(z_k, t_m)$  can be used to evaluate the overall performance for  
217 the whole depths.

218 Figure 5 a and b show the vertical distribution of [H-RMSEs<sup>\(T\)</sup>](#) for  $t_1=24$ -hour and  
219  $t_2=168$ -hour forecasts with and without Argo profiles assimilation. Since the high  
220 resolution and horizontally uniform satellite remote sensing SST data are assimilated,  
221 inclusion of Argo data does not improve the accuracy of SST prediction.

222 [H-RMSEs<sup>\(T\)</sup>](#) at time  $t_1$  and  $t_2$  increase with depth from the surface to its  
223 maximum value at around 158 m depth, where is the mean thermocline location,  
224 reduce drastically to  $0.5^\circ\text{C}$  at around 1000 m depth, and reduce gradually to  $0.25^\circ\text{C}$

225 to 2000 m depth. The low value of  $H\text{-RMSE}^{(T)}$  below 1000 m depth for all cases may  
226 be caused by the low variability.

227 For 24-hour forecast (Fig. 5a), the maximum value of  $H\text{-RMSE}^{(T)}$  is  $2.1^{\circ}\text{C}$   
228 without Argo data assimilation and  $1.6^{\circ}\text{C}$  with Argo data assimilation (24% error  
229 reduction). The improvement of ocean prediction is very evident until 1000 m depth.  
230 Since the value of  $H\text{-RMSE}^{(T)}$  below 1000 m depth is already small ( $0.25\text{--}0.5^{\circ}\text{C}$ ), the  
231 improvement with the Argo data is not noticeable. Such improvement in upper 1000  
232 m especially at around 158 m depth is still evident in 168-hour forecast (Fig. 5b).



233  
234 Figure 5 c and d show the vertical distribution of  $H\text{-RMSEs}^{(S)}$  for  $t_1=24\text{-hour}$  and  
235  $t_2=168\text{-hour}$  forecasts with and without Argo profile data assimilation. Similar to the  
236 temperature prediction, the  $H\text{-RMSE}$  of salinity for all cases reduces evidently from  
237 the surface to depth around 1200 m, and reduces gradually below 1200 m. The low  
238 value of  $H\text{-RMSE}^{(S)}$  below 1200 m depth is related to the low variability. Without  
239 Argo data assimilation,  $H\text{-RMSEs}^{(S)}$  at time  $t_1$  and  $t_2$  are very large, with more than  
240 0.5 psu for depths shallower than 300 m. With Argo data assimilation, they decrease  
241 drastically to less than 0.23 psu for 24-hours forecast and 0.25 psu for 168-hour  
242 forecast with error reduction more than 50%. Below 1200 m depth,  $H\text{-RMSEs}^{(S)}$  at  
243 time  $t_1$  and  $t_2$  are quite small with slightly larger values in “WITH\_ARGO”  
244 experiment than in the “NO\_ARGO” experiment. This may be related that the depth  
245 of assimilating data is limited to upper 1000m. A further study is needed to explain  
246 such phenomena.

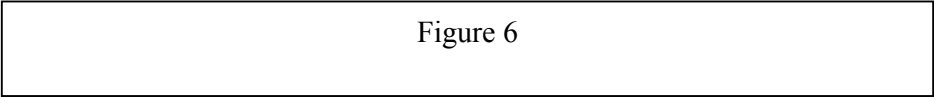
247 **4.2 Near Thermocline**

248 The mean errors (ME) within the layers between  $z_{k1}$  and  $z_{k2}$  at time  $t_m$  is  
249 calculated using Eq.(3) to identify the forecast system performance.

250 
$$ME_{k_1, k_2}^{(\psi)}(x_n, y_n, t_m) = \frac{1}{K} \sum_{k=k_1}^{k_2} (\psi^p(x_n, y_n, z_k, t_m) - \psi^o(x_n, y_n, z_k, t_m)) \quad (3)$$

251 Where all letters express the same means as ones in the Eq.(2) and  $k_1, k_2$  represents  
252 the  $k_1$ th and  $k_2$ th level, respectively; K equals to  $k_1-k_2$ . Here, to evaluate the forecast  
253 performance near the mean thermocline, the depths of the  $k_1$ th and  $k_2$ th level are 100m  
254 and 300m, respectively, and the  $t_m$  is 24-hour.

255 Figure 6 a and b show the horizontal distributions of the vertically (100-300 m)  
256 averaged temperature mean errors in 24-hour forecast without and with Argo data  
257 assimilation, respectively. Without Argo data assimilation, the predicted temperatures  
258 are lower than observations in most areas. In the east areas of Japan, the predicted  
259 temperatures are 0.8°C higher than observations. With Argo data assimilation, the  
260 predicted temperatures are significantly improved, and the forecast errors are 0.1°C  
261 or less in the whole areas. Therefore, the assimilation of Argo data can reduce errors  
262 of temperature forecast dramatically near the mean thermocline.



264 Figure 6 c and d show the horizontal distributions of the vertically (100-300 m)  
265 averaged salinity mean errors in 24-hour forecast without and with Argo data  
266 assimilation, respectively. Without Argo data assimilation, the predicted salinity is  
267 significantly lower than observations in most areas. For example, the predicted

268 salinity is over 0.5 psu lower than observation in the area of 15°N-35°N. However, the  
 269 predicted salinity is significantly higher than observation in the small east area of  
 270 Japan. It indicates that an obvious bias exists for salinity forecast without Argo data  
 271 assimilation. With Argo data assimilation, the predicted salinity is significantly  
 272 improved, and the forecast errors are 0.2 psu or less in the whole areas. Therefore, the  
 273 assimilation of Argo data can reduce errors of salinity forecast dramatically near the  
 274 mean halocline.

### 275 **4.3 Error Evolution**

276 The **spatially averaged root mean square error (S-RMSE)** between predicted and  
 277 observed values for the whole horizontal region within the layers between  $z_{k1}$  and  $z_{k2}$   
 278 and at time  $t_m$ ,

$$279 \quad \text{S-RMSE}_{k_1, k_2}^{(\psi)}(t_m) = \sqrt{\frac{1}{NK} \sum_{k=k_1}^{k_2} \sum_{n=1}^N [\psi^p(x_n, y_n, z_k, t_m) - \psi^o(x_n, y_n, z_k, t_m)]^2} \quad (4)$$

280 is also used for the evaluation. Just as Eq.(3), all letters in the Eq.(4) express the same  
 281 means as ones in the Eq.(2).

282 The **S-RMSEs** of temperature are calculated using Eq.(4) for upper (0–50m) and  
 283 lower (50–1000m) layers to analysis the errors growth (Fig. 7). The **S-RMSEs<sup>(T)</sup>** are  
 284 generally lager and grow faster in the upper layer than in the lower layer. For the  
 285 upper layer, without Argo data assimilation, the **S-RMSE<sup>(T)</sup>** is 1.33°C for 24-hour  
 286 forecast, and 1.51°C for 168-hour forecast (14% increasing). With Argo data  
 287 assimilation, the **S-RMSE<sup>(T)</sup>** is 1.26°C for 24-hour forecast, and 1.49°C for 168-hour  
 288 forecast (18% increasing). For the lower layer, without Argo data assimilation, the



289  $S\text{-RMSE}^{(T)}$  is  $1.15^{\circ}\text{C}$  for 24-hour forecast, and  $1.18^{\circ}\text{C}$  for 168-hour forecast (3%  
290 increasing). With Argo data assimilation, the  $S\text{-RMSE}^{(T)}$  is  $0.93^{\circ}\text{C}$  for 24-hour  
291 forecast, and  $1.03^{\circ}\text{C}$  for 168-hour forecast (11% increasing).

292 With Argo data assimilation, the accuracy of temperature forecasts is  
293 significantly improved. However, it is worthy note that the forecast errors in the  
294 “WITH\_ARGO” experiment grow a little faster compared to those in the  
295 “NO\_ARGO” experiment. This is because the assimilation of Argo data just improves  
296 the accuracy of initial conditions and can not correct the model systematic bias. As a  
297 result, the forecast error around initial forecast time in the “WITH\_ARGO”  
298 experiment is mainly determined by the accuracy of initial conditions and much lower  
299 than ones in the “NO\_ARGO” experiment, and with the increase of the forecast time,  
300 the forecast error is mainly affected by model systematic bias so that the forecast error  
301 with assimilation of Argo data increases sharply.

Figure 7, 8

302  
303 Same as the temperature, the  $S\text{-RMSEs}$  of salinity are calculated using Eq.(4) for  
304 upper (0–300m) and lower (300–1000m) layers to identify the errors growth (Fig. 8).  
305  $S\text{-RMSEs}^{(S)}$  are generally lager in the upper layer than in the lower layer. For the  
306 upper layer, without Argo data assimilation, the  $S\text{-RMSE}^{(S)}$  is near 0.5 psu for the  
307 whole prediction period. With Argo data assimilation, the  $S\text{-RMSE}^{(S)}$  is 0.17 psu for  
308 24-hour forecast, and 0.22 psu for 168-hour forecast, much less than 50% of that  
309 without Argo data assimilation. For the lower layer, without Argo data assimilation,  
310 the  $S\text{-RMSE}^{(S)}$  is near 0.15 psu for the whole prediction period. With Argo data

311 assimilation, the  $S\text{-RMSEs}^{(S)}$  are 0.07 psu and 0.09 psu for 72-hour and longer  
312 forecast, and the  $S\text{-RMSEs}^{(S)}$  reduce around 40% relative to that without Argo data  
313 assimilation. So, with Argo data assimilation, the accuracy of salinity forecasts is  
314 significantly improved.

315 

Figures 9
-----------

#### 316 **4.4 Vertical Cross Sections**

317 A set of CTD temperature measurements (not being used in the data assimilation)  
318 is used for the evaluation. It was conducted on 23 February 2008 along 129°E south  
319 of Japan. Figure 9a gives the distribution of observational temperatures for the 129°E  
320 cross-section, while Fig. 9b and c show results of 24-hour forecast for both  
321 experiments. Temperature field with Argo data assimilation is closer to observations  
322 than that without Argo data assimilation.

323 The section along 38.5°E east of Japan during 8 May 2008 is used for illustration.  
324 Figure 10a gives the distribution of observational salinity, while Fig. 10b and c show  
325 results of 24-hour forecast for both experiments. Just as temperature section, salinity  
326 field with Argo data assimilation is closer to observations than that without Argo data  
327 assimilation.

#### 328 **5. Conclusion**

329 A forecast system based on the Princeton Ocean Model with generalized  
330 coordinate system (POMgcs) and sequential multi-grid 3DVAR analysis scheme is

331 developed for the western Pacific marginal seas to investigate the impact of sampling  
332 strategies on the ocean prediction through using two ( $T$ ,  $S$ ) profile datasets. The first  
333 dataset contains both conventional and Argo profile data (called “WITH\_ARGO”)  
334 and represents horizontally uniform (relative) sampling. The second dataset contains  
335 only the conventional profile data (called “NO\_ARGO”) and represents horizontally  
336 non-uniform sampling.

337       Without Argo data assimilation (i.e., non-uniform sampling), temperature and  
338 salinity forecast have obvious biases. Especially in the area of 15°N-35°N the  
339 predicted temperature and salinity are obviously smaller than observations. With Argo  
340 data assimilation, these biases are corrected. Based on the detailed comparison of  
341 horizontally averaged root mean square error (H-RMSE) between the two  
342 experiments, it is known that the temperature H-RMSE maximum drops by 24% and  
343 the salinity H-RMSEs in depth shallower than 300m drop averagely by 50% if the  
344 Argo data is assimilated into initial fields, and the accuracy of salinity forecast is  
345 improved more obviously than temperature forecast. With Argo data assimilation, the  
346 temperature or salinity distribution along some vertical cross sections is nearer to  
347 observations than that without Argo data assimilation. It indicates that the assimilation  
348 of Argo data plays an important role in the process of constructing initial fields, and it  
349 can significantly improves the temperature and salinity forecasts. It is worthy note that  
350 although the forecast errors within assimilation depth (shallower than 1000m) can be  
351 sharply reduced though assimilating Argo data into initial filed, the errors below  
352 1000m depth change very small, or even can slightly increase. A further study is

353 needed to explain such phenomena.

## 354 **Acknowledgements**

355 This study was jointly supported by grants of the National Natural Science  
356 Foundation of China (41030854, 40906015, 40906016, 41106005, and 41176003,  
357 41206178), and National Science and Technology Support program  
358 (2011BAC03B02-01-04).

## 359 **Reference**

- 360 Chu Peter C, Wang GuiHua, Fan Chenwu. 2004. Evaluation of the U.S. Navy's  
361 Modular Ocean Data Assimilation System (MODAS) using the South China Sea  
362 Monsoon Experiment (SCSMEX) data. *J. Oceanogr.*, **60**: 1007-1021
- 363 Chu Peter C, Amezaga G R, Gottshall E L, et al. 2007a. Ocean nowcast/forecast  
364 systems for improvement of Naval undersea capabilities. *Marine Technol. Soc. J.*,  
365 **41**(2): 23-30
- 366 Chu Peter C, Mancini S, Gottshall E L, et al. 2007b. Sensitivity of satellite altimetry  
367 data assimilation on weapon acoustic preset using MODAS. *IEEE J. Oceanic*  
368 *Eng.*, **32**: 453-468
- 369 Chu Peter C, Fan Chenwu. 2010. A conserved minimal adjustment scheme for  
370 stabilization of hydrographic profiles. *J. Atmos. Oceanic Technol.*, **27**(6):  
371 1072-1083
- 372 Galanis G, Chu Peter C, Kallos G. 2011. Statistical post processes for the

373 improvement of the results of numerical wave prediction models. A combination  
374 of Kolmogorov-Zurbenko and Kalman filters. *J. Operat. Oceanogr.*, **4**(1): 23-31

375 Griffa A, Molcard A, Raicich F, et al. 2006. Assessment of the impact of TS  
376 assimilation from ARGO floats in the Mediterranean Sea. *Ocean Sci.*, **2**: 237-248

377 Han Guijun, Li Wei, Zhang Xuefeng, et al. 2011. A regional ocean reanalysis system  
378 for China coastal waters and adjacent seas. *Advances in Atmospheric Sciences*,  
379 **28**(3): 682-690

380 He Zhongjie, Han Guijun, Li Wei, et al. 2010. Experiments on assimilating of satellite  
381 data in the China seas and adjacent seas (in Chinese). *Periodical of Ocean*  
382 *University of China*, **40**(9): 1-7

383 Li Wei, Xie Yuanfu, He Zhongjie, et al. 2008. Application of the multi-grid data  
384 assimilation scheme to the China Seas' temperature forecast. *J. Atmos. Oceanic*  
385 *Technol.*, **25**(11): 2106-2116

386 Li Wei, Xie Yuanfu, Deng Shiohming, et al. 2010. Application of the multigrid  
387 method to the two-dimensional doppler radar radial velocity data assimilation. *J.*  
388 *Atmos. Oceanic. Tech.*, **27**(2): 319-332

389 Liu Yimin, Zhang Renhe, Yin Yonghong, et al. 2004. The Application of ARGO Data  
390 to the Global Ocean Data Assimilation Operational System of NCC. *Acta*  
391 *Meteorologica Sinica*, **19**: 355-365

392 Marshall J, Hill C, Perelman L, et al. 1997. Hydrostatic, quasi-hydrostatic, and  
393 nonhydrostatic ocean modelling. *J. Geophys. Res.*, **102**(C3): 5733-5753

394 Troccoli A, Balmaseda M A, Segschneider J, et al. 2002. Salinity adjustments in the

395 presence of temperature data assimilation. *Mon. Wea. Rev.*, **130**: 89-102

396 Wong A P S, Johnson G C, Owens W B. 2003. Delayed-mode calibration of  
397 autonomous CTD profiling float salinity data by  $S-\theta$  climatology. *J. Atmos.*  
398 *Oceanic Tech.*, **20**:308-318

399 Zhu Jiang, Yan Changxiang. 2006. Nonlinear balance constraints in 3DVAR data  
400 assimilation. *Science in China (D)*, **49**: 331-336

401

402

403

404

405

406

407

408

409

410

411

412

413

414

415

416 **Figure**

417 Fig. 1. Geography of the Western North Pacific. The dots indicate the numerical grid  
418 points.

419 Fig. 2. Spatial distribution of temperature (a) and salinity (b) profiles from GTSP  
420 during Jan-Dec 2008 (Red dot: conventional data; Blue dot: Argo data).

421 Fig. 3. Vertical distributions of numbers of observations for temperature (red) and  
422 salinity (blue) from conventional (a) and Argo data (b).

423 Fig. 4. Flow chart of multi-grid 3DVAR operational procedure.

424 Fig. 5. Vertical dependence of temperature (a, b, □) and salinity (c, d, psu) **H-RMSEs**  
425 in 24-hour forecast (a, c) and 168-hour forecast (b, d) with and without Argo data  
426 assimilation.

427 **Fig. 6.** Horizontal distribution of vertically (100-300 m) averaged temperature (a, b,  
428 °C) and salinity (c, d, psu) prediction errors in 24-hour forecast without Argo profiles  
429 assimilation(a, c) and with Argo profiles assimilation(b, d).

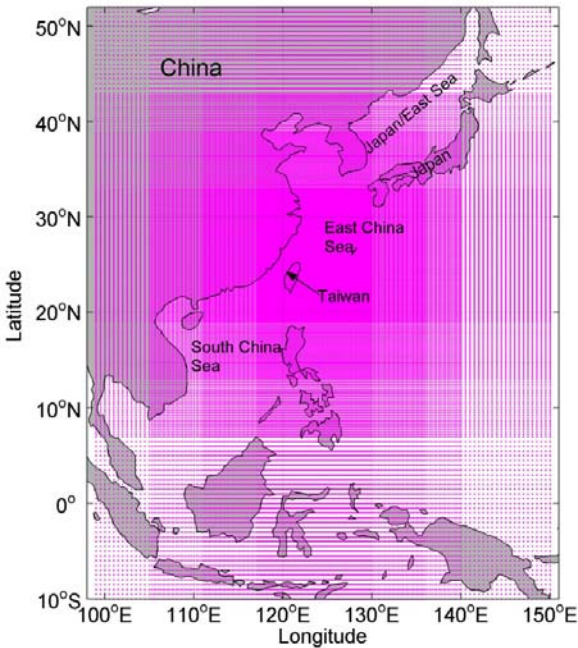
430 **Fig. 7.** Temporal variation of **temperature S-RMSEs** (°C) for the layers of 0-50m(a)  
431 and 50-1000m(b) in 24-hour forecast with and without Argo data assimilation.

432 **Fig. 8.** Temporal variation of **salinity S-RMSEs** (psu) for the layers of 0-300m(a) and  
433 300-1000m(b) in 24-hour forecast with and without Argo data assimilation.

434 **Fig. 9.** Vertical temperature cross-section along 129°E south of Japan on 23 February  
435 2008: (a) observation (dark dots: stations), (b) 24-hour forecast without assimilating  
436 Argo profiles, and (c) 24-hour forecast with assimilating Argo profiles.

437 **Fig. 10.** Vertical salinity cross-section along 38.5°N east of Japan on 8 May 2008: (a)  
438 observation (dark dots: stations), (b) 24-hour forecast without assimilating Argo  
439 profiles, and (c) 24-hour forecast with assimilating Argo profiles.

440



441

442 Fig. 1. Geography of the Western North Pacific. The dots indicate the numerical grid  
443 points.

444

445

446

447

448

449

450

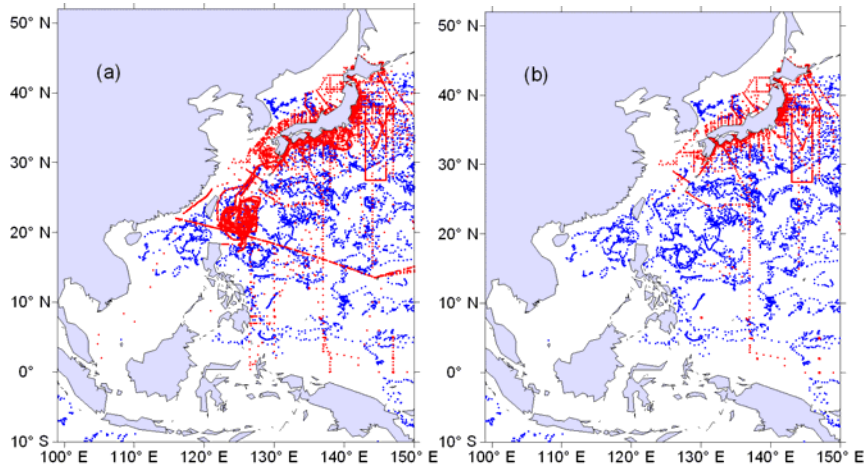
451

452

453

454





455

456 Fig. 2. Spatial distribution of temperature (a) and salinity (b) profiles from GTSPP

457 during Jan-Dec 2008 (Red dot: conventional data; Blue dot: Argo data).

458

459

460

461

462

463

464

465

466

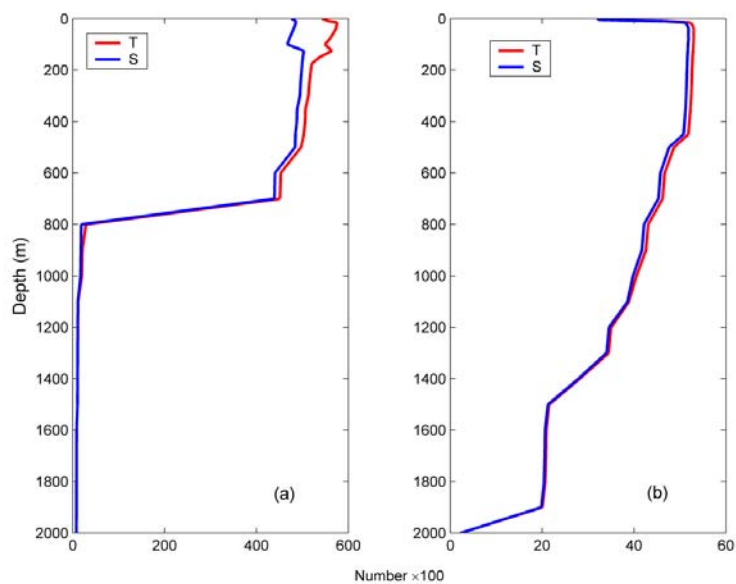
467

468

469

470

471



472

473 Fig. 3. Vertical distributions of numbers of observations for temperature (red) and  
 474 salinity (blue) from conventional (a) and Argo data (b).

475

476

477

478

479

480

481

482

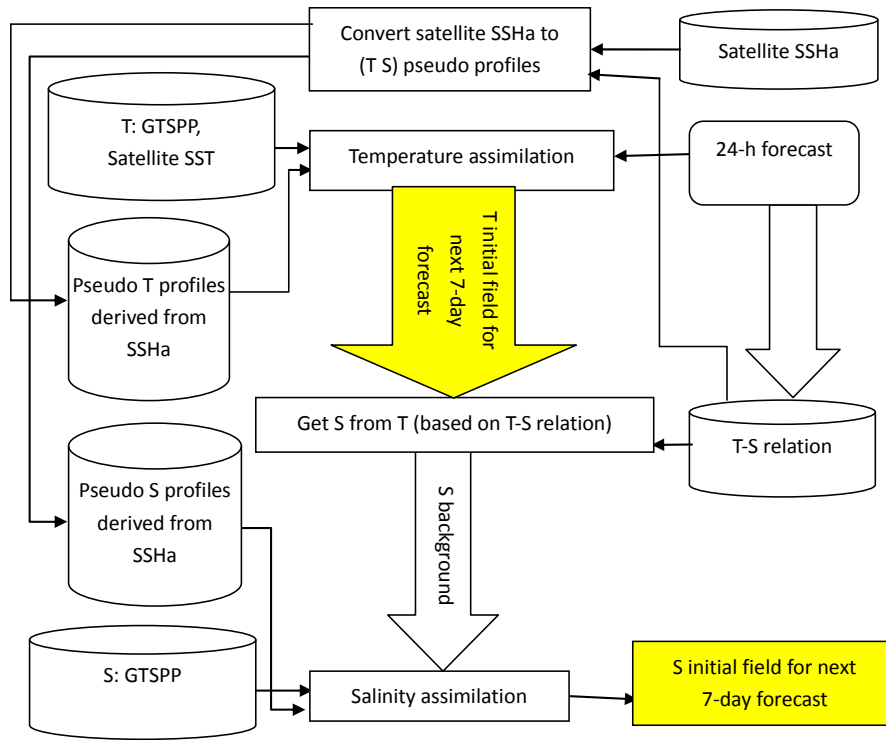
483

484

485

486

487



488

489 Fig. 4. Flow chart of multi-grid 3DVAR operational procedure.

490

491

492

493

494

495

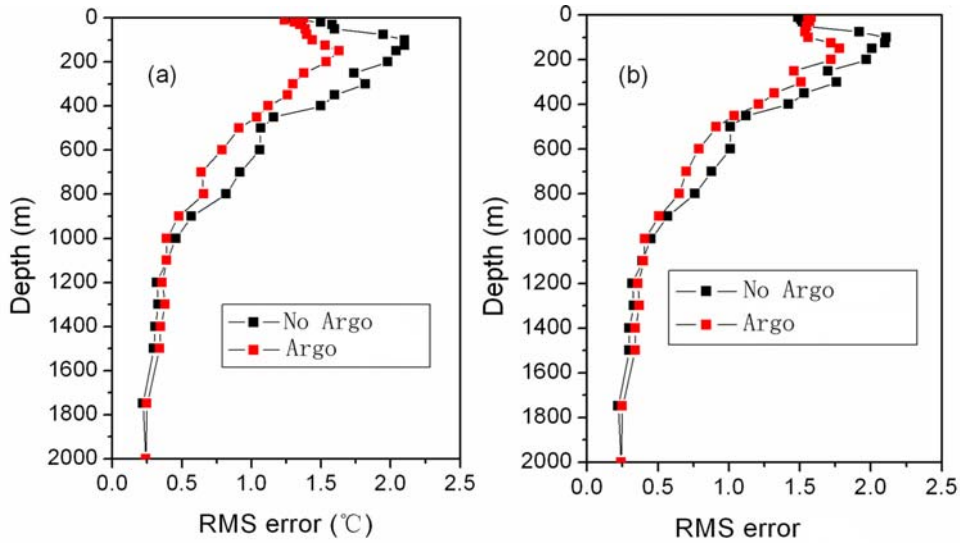
496

497

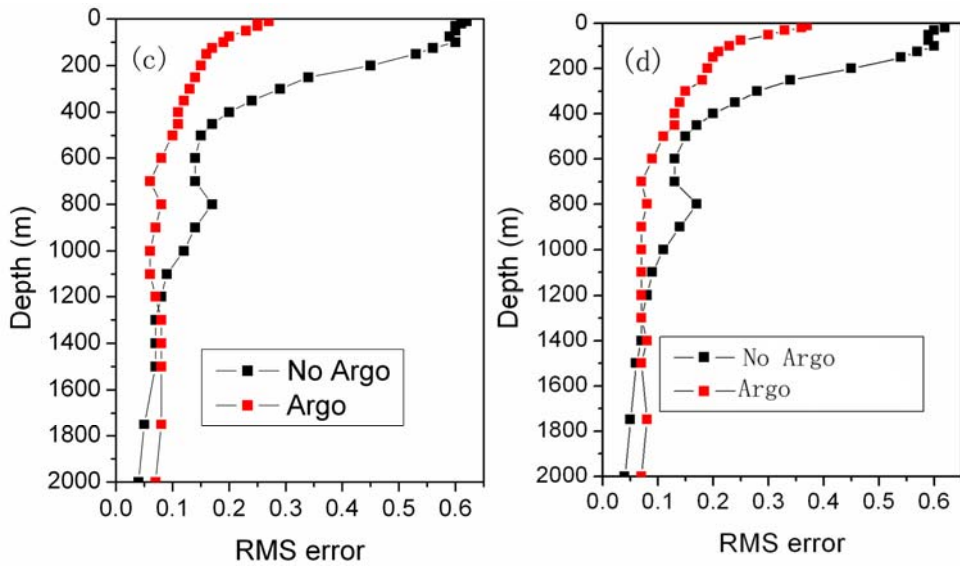
498

499

500



501



502

503 Fig. 5. Vertical dependence of temperature (a, b, □) and salinity (c, d,  $\square$ ) H-RMSEs

504 in 24-hour forecast (a, c) and 168-hour forecast (b, d) with and without Argo data

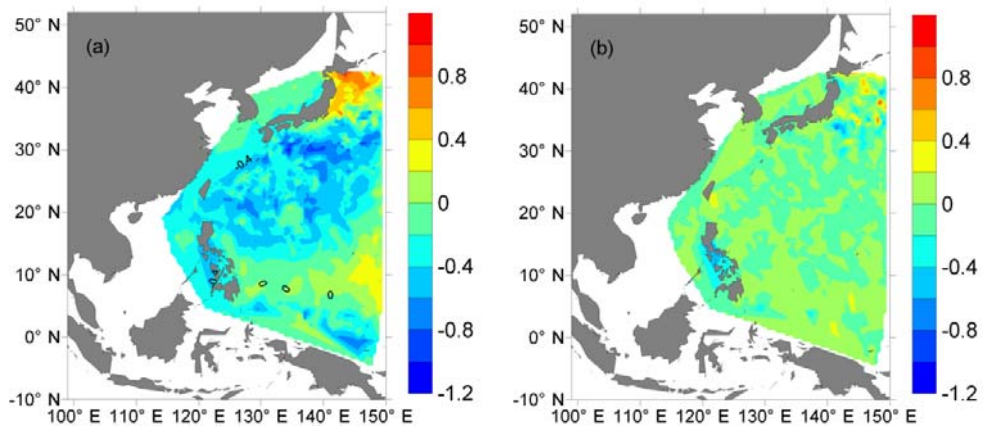
505 assimilation.

506

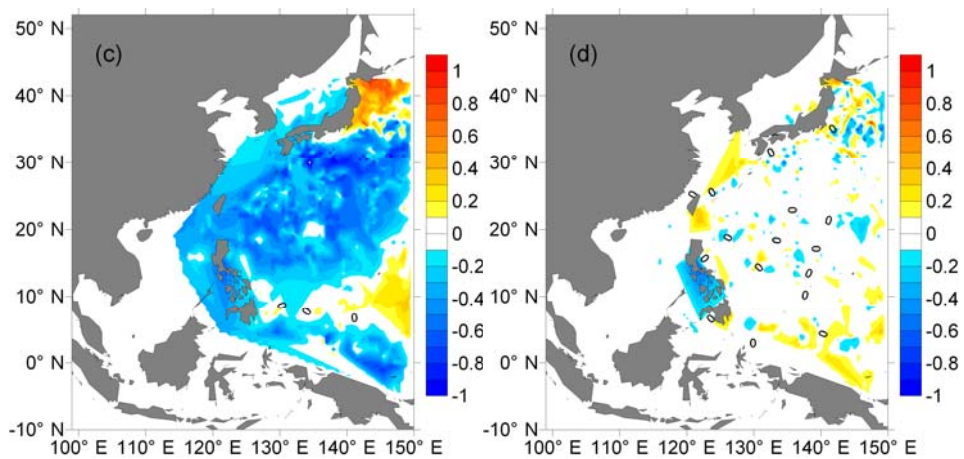
507

508

509



510



511

512 **Fig. 6.** Horizontal distribution of vertically (100-300 m) averaged temperature (a, b,  
513 °C) and salinity (c, d, psu) prediction errors in 24-hour forecast without Argo profiles  
514 assimilation(a, c) and with Argo profiles assimilation(b, d).

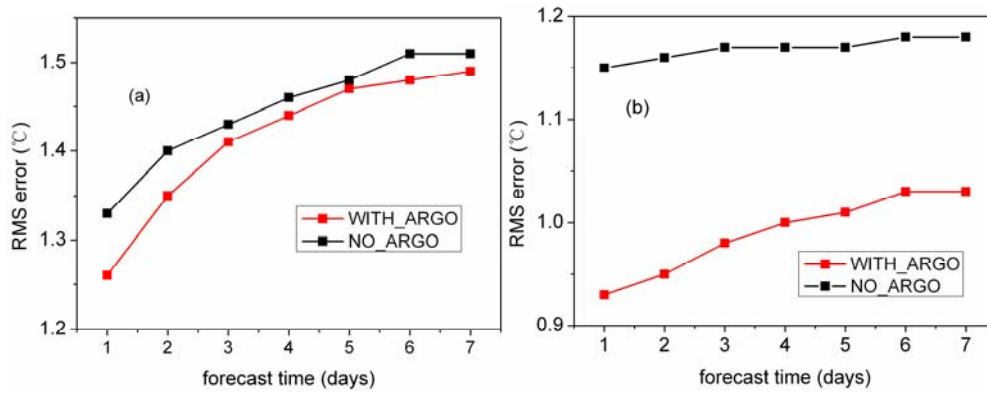
515

516

517

518

519



520

521 **Fig. 7.** Temporal variation of [temperature S-RMSEs](#) (°C) for the layers of 0-50m(a)

522 and 50-1000m(b) in 24-hour forecast with and without Argo data assimilation.

523

524

525

526

527

528

529

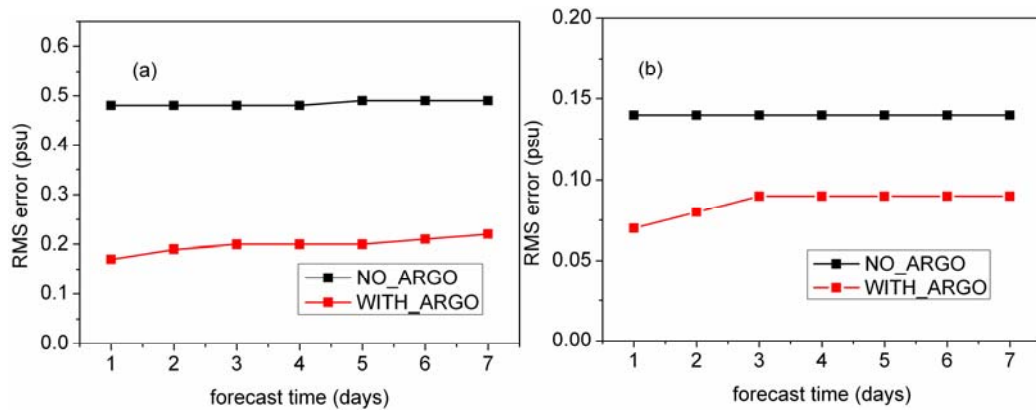
530

531

532

533

534



535

536 **Fig. 8.** Temporal variation of salinity S-RMSEs (psu) for the layers of 0-300m(a) and

537 300-1000m(b) in 24-hour forecast with and without Argo data assimilation.

538

539

540

541

542

543

544

545

546

547

548

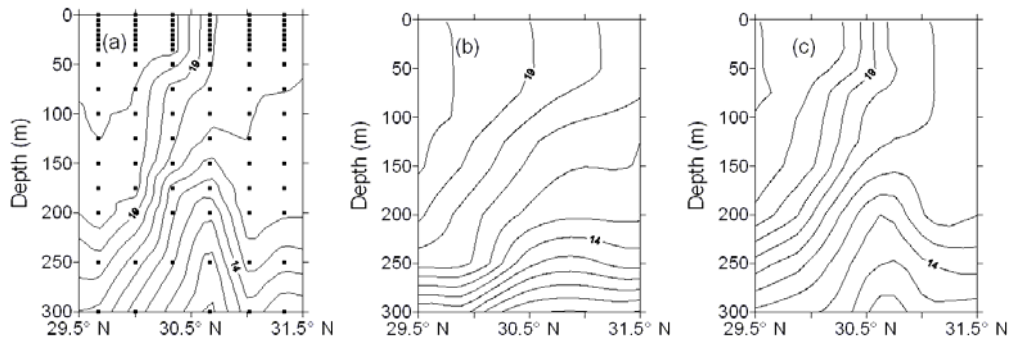
549

550

551

552

553



554

555 **Fig. 9.** Vertical temperature cross-section along 129°E south of Japan on 23 February  
 556 2008: (a) observation (dark dots: stations), (b) 24-hour forecast without assimilating  
 557 Argo profiles, and (c) 24-hour forecast with assimilating Argo profiles.

558

559

560

561

562

563

564

565

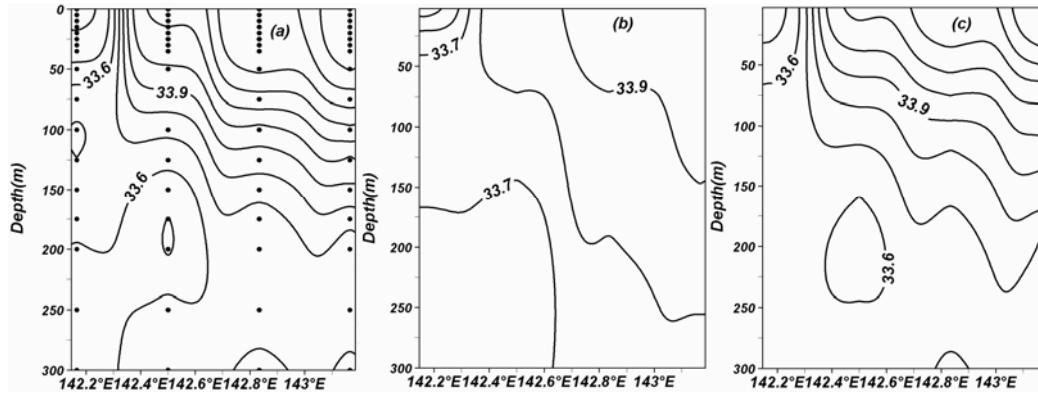
566

567

568

569





570

571 **Fig. 10.** Vertical salinity cross-section along 38.5°N east of Japan on 8 May 2008: (a)  
 572 observation (dark dots: stations), (b) 24-hour forecast without assimilating Argo  
 573 profiles, and (c) 24-hour forecast with assimilating Argo profiles.

574

575